1 **Mass independent fractionation of even and odd mercury isotopes during free tropospheric mercury**

2 **oxidation**

3

4 Xuewu Fu[1,2], Martin Jiskra[1,3], Xu Yang[1,2], Nicolas Marusczak[1], Maxime Enrico[1,$], Jerome Chemleff[1], Lars-

5 Eric Heimbürger[1,%] François Gheusi[4], Jeroen E. Sonke[1,*]

6

7 [1] Géosciences Environnement Toulouse, CNRS/IRD/CNRS/Université de Toulouse, France

8 [2] State Key Laboratory of Environmental Geochemistry, Institute of Geochemistry, Chinese Academy of

9 Sciences, Guiyang, 550081, China.

10 [3] Environmental Geosciences, University of Basel, Switzerland

11 [4] Laboratoire d'Aérologie, CNRS/IRD/Université de Toulouse, France

12 [$] present address: Harvard John A. Paulson School of Engineering & Applied Sciences, Harvard University,

13 Cambridge, MA, USA

14 [%] present address: Mediterranean Institute of Oceanography, Aix Marseille Université, CNRS/IRD, Université

15 de Toulon, IRD, Marseille, France

16

17 * Corresponding Author: jeroen.sonke@get.omp.eu

18

19

20

21

22

23

24

25

26

Abstract. Even mercury (Hg) isotope mass independent fractionation (MIF), observed in rainfall globally, is used to quantify atmospheric Hg deposition pathways. The underlying reaction and MIF mechanism are unknown however. Here we investigate the Hg isotope composition of free tropospheric gaseous elemental Hg^0 and Hg^{II} forms. We find that gaseous oxidized Hg^{II} has positive $\Delta^{199}Hg$, $\Delta^{201}Hg$, $\Delta^{200}Hg$, and negative $\Delta^{204}Hg$ signature, similar to rainfall Hg^{II}, and we document rainfall Hg^{II} $\Delta^{196}Hg$ to be near-zero. Cloud water and rainfall Hg^{II} show enhanced odd MIF compared to gaseous Hg^{II}, indicating in-cloud Hg^{II} photoreduction. Hg MIF observations of free tropospheric Hg^0 dynamics show how net Hg^0 oxidation leads to opposite MIF in Hg^0 and Hg^{II}. A $\Delta^{200}Hg$ mass balance for Hg^0 and Hg^{II} forms suggests that measurements and models underestimate the tropospheric Hg^{II} pool.

Introduction

Modern anthropogenic Hg emissions (2400 Mg a^{-1}) outweigh natural Hg emissions by an order of magnitude (Bagnato et al., 2014; Streets et al., 2019). Hg emissions are mostly in the form of gaseous elemental Hg (GEM), which has a long atmospheric life-time against oxidation to divalent reactive Hg (RM) forms that include gaseous oxidized Hg (GOM) and particulate bound Hg (PBM) (Amos et al., 2012). RM is rapidly deposited to continental and marine ecosystems where microbial activity transforms inorganic Hg into the bioaccumulating and toxic methylmercury form (Fitzgerald and Lamborg, 2004). Predicting the impact of anthropogenic Hg emission scenarios on global Hg deposition requires detailed understanding of atmospheric Hg transformations and of GEM oxidation in particular. Two decades of atmospheric Hg research using mountain-top and in-flight observations, experimental and theoretical reaction kinetics, and coupled 3D atmosphere-ocean chemistry and transport models, have given broad understanding of atmospheric Hg dynamics (Ariya et al., 2015; Dibble et al., 2020; Donohoue et al., 2006; Holmes et al., 2010; Seigneur et al., 2004). Experimental, theoretical and modeling studies suggest Hg oxidation initiated by bromine (Br) radicals to be faster than by ozone or OH (Horowitz et al., 2017; Wang et al., 2014), yet major uncertainties in RM concentrations, oxidation and reduction mechanisms and rates remain (Jaffe et al., 2014; Saiz-Lopez et al., 2018; Weiss-Penzias et al., 2015).

Hg stable isotope analysis of atmospheric Hg compounds may provide new information on Hg emission sources and complex atmospheric redox cycling. During the last decade, significant advances have been made in the measurement of Hg isotope compositions of biogeochemical reservoirs (Kwon et al., 2020). Laboratory and field evidence suggests that processes controlling Hg emission such as reduction/oxidation, adsorption/desorption, or volatilization can induce significant mass dependent Hg isotope fractionation (MDF,

57 $\delta^{202}Hg$ signature)(Jiskra et al., 2015; Kritee et al., 2012; Wiederhold et al., 2010). Large mass independent Hg

58 isotope fractionation (MIF) of odd Hg isotopes by the magnetic isotope effect has been observed in aqueous

59 photochemical Hg reduction experiments ($\Delta^{199}Hg$, $\Delta^{201}Hg$ signatures) (Bergquist and Blum, 2007; Zheng and

60 Hintelmann, 2009). Odd-MIF signatures imparted on inorganic Hg and methyl-Hg by photochemistry can be

61 traced into all Earth surface environments, i.e sediments, biota, atmosphere, soils etc. Unusual even isotope MIF

62 ($\Delta^{200}Hg$, $\Delta^{204}Hg$) has been observed in rainfall and snowfall globally (Chen et al., 2012; Demers et al., 2013;

63 Gratz et al., 2010), and has been speculated to originate in GEM photo-oxidation at and above the tropopause

64 (Chen et al., 2012). The exact even-MIF mechanism and even-MIF inducing Hg transformation(s) remain

65 essentially unknown.

66 In this study we investigate Hg isotope composition of GEM, RM, and cloud water at the high altitude Pic

67 du Midi Observatory (PDM, 2877m, France). The PDM regularly receives free tropospheric air masses that are

68 enriched in RM and depleted in GEM (Fu et al., 2016a). High frequency, 12h and 24h GEM isotope observations

69 of a free tropospheric air mass rich in GOM and depleted in GEM are investigated to derive MDF and MIF

70 factors for net oxidation. Photoreduction experiments on rainfall are made to constrain atmospheric aqueous

71 MDF and MIF factors. Finally, we investigated the even-MIF on the low abundance ^{196}Hg isotope to help

72 understand potential even-MIF mechanisms.

73

74 **Materials and methods**

75 **Site description and ancillary parameters**

76 The Pic du Midi Observatory (PDM, 0.14º E, 42.94º N, 2877 m a.s.l) is a high-altitude monitoring station

77 situated on top of an isolated peak on the north edge of the central Pyrenees Mountains, Southwest France. The

78 PDM receives free tropospheric air from the Northeast Atlantic Ocean and Europe and boundary layer air from

79 upslope winds in Spain and southwest France (Gheusi et al., 2011; Hulin et al., 2019). The station receives

80 predominantly southerly and southwesterly winds (> 70 %) across the main range of Pyrenees (Hulin et al.,

81 2019). There are no major anthropogenic Hg emission point sources around the station or in the surrounding

82 areas.

83

84 **Atmospheric sampling and processing**

85 Short-term (12/24h) variations in atmospheric GEM isotopic composition were investigated from 19 to 28 in

86 Dec 2012 at PDM using large chlorine-impregnated activated carbon (CLC) traps. Traps with 600 mg CLC were

87   utilized for 24 hour sampling at a flow rate of ~ 10 L min^{-1}; whereas traps with 1000 mg of CLC were utilized

88   for 12 hour sampling at a flow rate of ~ 20 LPM (Fu et al., 2014). The sampling inlets of the CLC traps (heated

89   at 70°C to avoid water condensation), preceded by a pre-burned 47mm quartz fiber filter were connected to a

90   Tekran 1104 Teflon coated sampling manifold, operating at 100 LPM and 70°C, and installed into the prevailing

91   wind direction. Sampling flow rates of CLC traps were regulated via ball flow meters installed at the outlets of

92   the vacuum pumps, and the total sampling volumes of the traps were recorded using gas meters. Similar to

93   Arctic studies (Berg et al., 2013; Steffen et al., 2005) we find that the Hg collected on CLC traps reflects the

94   GEM fraction, and is not confounded by the GOM fraction. Both GOM and PBM fractions are retained on the

95   quartz filter preceding the CLC trap. Quartz has been previously shown to efficiently scavenge GOM over time

96   periods shorter than 24h (Lyman and Jaffe, 2011; Lynam and Keeler, 2002). CLC traps were thermally

97   decomposed (25°C to 1000°C over 8h) in a Hg-free oxygen flow (25 ml min^{-1}) in a tube furnace. Combustion

98   products were further decomposed in a 2nd pyrolizer tube furnace at 1000°C, and purged into a 10 ml 40 vol%

99   2HNO$_3$/1HCl oxidizing solution (Sun et al., 2013). CLC sampling efficiencies were better than 95%, mean

100   recovery efficiencies were 87%, and full procedural blanks <2% of Hg concentrations in trapping solutions (Fu

101   et al., 2014).

102   Twelve samples of the atmospheric RM (RM=GOM+PBM) were obtained using Millipore

103   polyethersulfone cation exchange membranes (CEMs, Millipore, 0.45 µm pore size, 47 mm and 90 mm diameter

104   (Maruszczak et al., 2017)) at the PDM from June to October 2014, with sampled air volumes between 25 and 77

105   m^3. Cloud water samples were collected from July to November 2014 with a CASCC-2 sampler at the PDM

106   (Demoz et al., 1996). Rainfall was sampled from July to August 2014 150km downwind from the PDM at 800m

107   altitude in the Pyrenees foothills using acid-washed polypropylene buckets and reported elsewhere (Enrico et

108   al., 2016). Snowfall and rainfall was collected at the PDM and the Geosciences Environnement Toulouse (GET,

109   Toulouse, France, 43.54° N, 1.48° E) laboratory between 2016 and 2017 using the same methods. Cloud water,

110   rainfall and snowfall samples collected after each event were transferred into pre-cleaned Pyrex glass bottles (1

111   and 2 L volume), then oxidized by adding 0.1 – 1 % BrCl, and kept refrigerated before Hg concentration analysis

112   by CVAFS and further pre-concentration for Hg isotope analysis. Hg from rain and cloud water samples was

113   pre-concentrated by reducing and purging Hg with SnCl$_2$ and a clean argon flow and subsequent trapping in an

114   oxidizing solution, following Sherman, et al. (Sherman et al., 2012). Recoveries of procedural standards, rainfall

115   and cloud water samples was >95%. RM on CEMs was leached in 20 vol% 2HNO$_3$/1HCl with blanks <4% of

116   sampled RM.

117   Hg isotope fractionation factors during aqueous photochemical reduction of rainwater was studied using a

118   solar simulator (see (Yang et al., 2019) for details). A low Hg level (2.6 ng L^{-1}) rainfall sample 'GET rain 4'

119   obtained at GET was spiked with 103 ng L^{-1} NIST 3133 and equilibrated for 48 in the dark. A 450 mL aliquot

120   was then transferred into an acid-cleaned quartz reactor, and illuminated for 24h with the solar spectrum from

121   a Xe lamp. After 24, the 78 ng L^{-1} dissolved Hg(II) remaining in the 450mL reactor volume was transferred to

122   a pre-cleaned 1L Pyrex bottle, and pre-concentrated for Hg isotope analysis.

123

124   **Mercury isotopic analysis**

125   Hg isotope ratios were measured using cold vapor multi-collector inductively coupled plasma mass

126   spectrometry (CV-MC-ICPMS, Thermo-Finnigan Neptune, and Neptune Plus) at the Midi-Pyrenees

127   Observatory, Toulouse, France following the methods described in previous studies (Jiskra et al., 2019; Obrist

128   et al., 2017). Instrumental mass bias of MC-ICPMS was corrected by standard-sample-standard bracketing using

129   NIST3133 Hg at matching concentrations. Hg isotopic composition is reported in delta notation (δ) in units of

130   per mil (‰) referenced to the bracketed NIST 3133 Hg standard (Blum and Bergquist, 2007): $\delta^{xxx}Hg =$

131   $[(^{xxx}Hg/^{198}Hg)_{sample}/(^{xxx}Hg/^{198}Hg)_{NIST3133} -1]$, where xxx represent Hg isotope masses 199, 200, 201, 202, 204.

132   MIF values are expressed by "capital delta (Δ)" notation (‰), which is the difference between the measured

133   values of $\delta^{199}Hg$, $\delta^{200}Hg$, $\delta^{201}Hg$ and those predicted from $\delta^{202}Hg$ using the kinetic MDF law: $\Delta^{xxx}Hg$ (‰) =

134   $\delta^{xxx}Hg - (\beta^{xxx} \times \delta^{202}Hg)$, where β^{xxx} is -0.5074, 0.2520, 0.5024, 0.7520, 1.493 for the 196, 199, 200, 201, and 204

135   Hg isotopes respectively. The analytical uncertainty of isotopic analysis was assessed by repeated analysis of

136   the UM-Almaden and ETH-Fluka standards over different analysis sessions and at Hg concentrations

137   corresponding to the samples. The overall mean values of $\delta^{202}Hg$, $\Delta^{199}Hg$, $\Delta^{200}Hg$, $\Delta^{201}Hg$, and $\Delta^{204}Hg$ for all

138   the UM-Almaden standards in the 0.5 to 1.5 ng g^{-1} range were -0.56 ± 0.07 ‰, -0.04 ± 0.08 ‰, -0.01 ± 0.09 ‰

139   and -0.05 ± 0.09 ‰, and 0.04 ± 0.19 ‰ (2SD, n = 11) respectively, which agree well with previously reported

140   values (Blum and Bergquist, 2007). The procedural standard for rainfall pre-concentration, i.e. rainfall sample

141   'GET rain 4' spiked with 103 ng g^{-1} NIST 3133 showed good recovery and no isotopic bias (Supporting Data).

142   In the present study, the analytical uncertainty of CV-MC-ICPMS isotope analysis of RM, GEM, rainfall, and

143   snowfall is the 2SD uncertainty of the UM-Almaden standard, unless the 2SD uncertainty on repeated analysis

144   of the same sample over different analytical sessions was larger.

145   To attempt rainfall $\Delta^{196}Hg$ analysis, we screened rainfall samples obtained at GET in 2016 for both high

146   Hg concentration levels and high volume single events. Rainfall sample 'GET rain 6' was the only sample

147   retained as it consisted of a single thunderstorm event of 20.5 L, collected in the 8 large buckets, and had a Hg

148   concentration of 6.0 ng L^{-1}. The entire 20.5L volume was pre-concentrated 1200x in a single large Pyrex glass

149   bottle to a final concentration of 8.0 ng g^{-1} in 15.3 g of 20vol% iAR. The sample was run in duplicate during

150   two different days using dedicated UM-Almaden and ETH-Fluka standards, also at 8.0 ng g^{-1}. All individual

151   sample and standard results are given in the Supporting Data. The signals obtained on the ^{196}Hg and ^{202}Hg

152   isotopes during these sessions were 15mV and 3 Volt. We recommend the use of 10^{12} or 10^{13} Ω resistors on the

153   signal amplifier of the ^{196}Hg Faraday cup. The 2σ uncertainty, based on sample, UM-Almaden, and ETH-Fluka

154   replicates, on $\Delta^{196}Hg$ during these analysis sessions were 0.19‰ (Supplementary Data).

155

156   **Ancillary parameters**

157   Atmospheric Hg speciation at the PDM, including GEM, GOM and PBM, was continuously measured off

158   the same sampling manifold with a Tekran 2537/1130/1135 system (Tekran Inc., Canada) (Fu et al., 2016a;

159   Marusczak et al., 2017). Automated GOM and PBM analyses are subject to mounting criticism as the techniques

160   lack calibration, collection efficiency control and interference correction (Jaffe et al., 2014). We partly address

161   these issues by parallel manual sampling of RM (GOM + PBM) on CEMs (Huang et al., 2013). We find that

162   denuder-based GOM at the PDM is systematically underestimated by a factor of 1.56 for which we correct

163   (indicated by an asterisk hereafter, i.e. GOM*)(Marusczak et al., 2017). Atmospheric CO and O_3 concentrations

164   were continuously measured using a TEI (Thermo Environmental Instruments Inc. USA) 48CTL gas filter

165   correlation analyzer and 49C UV-absorption ozone analyzer, respectively, following published procedures

166   (Gheusi et al., 2011). Meteorology, CO and O3 data at the PDM were provided through the Pyrenean platform

167   for observation of the atmosphere (P2OA, http://p2oa.aero.obs-mip.fr).

168

169   **Air mass backward trajectories**

170   Seven day backward trajectories ending at PDM at a height of 3000 m above sea level were calculated

171   every 2 hours with simulated gridded meteorological data from the Weather Research and Forecasting (WRF)

172   model Version 3.4 with the Noah Land Surface Model, Thompson microphysics scheme, Grell-3 cumulus

173   scheme, Dudhia radiation physics scheme, YSU scheme for PBL. The modeled domain of meteorological data

174   mainly covered the eastern North Atlantic Ocean and European area, with a time resolution of 1 h, 400×800

175   grid cells at a 12-km horizontal resolution, and vertical levels of 50 from 1000 hPa to 20 hPa. All the trajectories

176   during the 12h, 24h of individual Hg isotope samples were grouped into an average backward trajectory to show

177   the mean air mass source region of samples.

178

179   **Results and discussion**

180   **GEM isotope compositions**

181   The nine day sampling period from 19 to 28 Dec 2012 was characterized by a shift from cloudy conditions (days

182   1-2, samples D1-D3) to clear skies (days 3-5, samples D4-D9), and back to clouds (days 7-9, samples D10-

183   D14). The wind direction was predominantly southwest bringing North-Atlantic Ocean air masses, over

184   northwest Spain, to the PDM. The continuous Hg speciation observations show a pronounced increase in GOM*

185   to 252 pg m^{-3} (48h mean), and concurrent decrease in GEM during samples D4-D6 (clear skies, Figure 1, Table

186   S1). Back trajectory analysis, and low observed relative humidity and CO, suggest that the high GOM event

187   represents the intrusion of a free tropospheric air mass that originated at 5000m (550hPa, Figures 1, 2). Such

188   intrusions are typical at PDM, e.g. 61 events were registered over a one year period from Nov 2011 to Nov 2012

189   (Fu et al., 2016a). The intrusions are of particular interest as they offer a snapshot of the free troposphere where

190   GEM oxidation is thought to take place (Fu et al., 2016a; Lyman and Jaffe, 2011; Swartzendruber et al., 2006;

191   Timonen et al., 2013). δ^{202}Hg, Δ^{199}Hg and Δ^{200}Hg of 12h and 24h GEM samples collected from 19 to 28 Dec

192   2012 were in the range of 0.16 to 0.51‰ (δ^{202}Hg, mean = 0.34‰), -0.31 to -0.11‰ (Δ^{199}Hg, mean = -0.23‰),

193   and -0.17 to 0.04‰ (Δ^{200}Hg, mean = -0.07‰) (Table S1). These observations are consistent with a single two-

194   week integrated GEM isotope sample B19, collected over the same period 19 to 28 Dec 2012 at a lower flow

195   rate of 2 L min^{-1}. with δ^{202}Hg of 0.39‰, Δ^{199}Hg of -0.27‰, Δ^{200}Hg of -0.10 ‰ (Fu et al., 2016b).

196

197   **RM, cloud water and rainfall Hg isotope compositions**

198   In a previous study we found that rainfall Hg isotope signatures 150km east from the PDM are typical of rainfall

199   observations globally, with a mean δ^{202}Hg 0.17 ± 0.33 ‰ and significantly positive odd MIF (Δ^{199}Hg = 0.72 ±

200   0.15 ‰; Δ^{201}Hg = 0.76 ± 0.14 ‰) and even-MIF (Δ^{200}Hg = 0.21 ± 0.04 ‰; Δ^{204}Hg = -0.33 ± 0.10 ‰, all 1σ, n

201   = 9) (Figure 3, Table S1, Enrico et al., 2016). Here we find that PDM cloud water THg concentrations and MDF

202   and MIF signatures are not significantly different from PDM and regional rainfall (p=0.26 to 0.79). For the first

203   time we observe that RM, i.e. GOM+PBM, at PDM also has positive odd MIF (Δ^{199}Hg = 0.44 ± 0.17 ‰; Δ^{201}Hg

204   = 0.44 ± 0.10 ‰) and even-MIF (Δ^{200}Hg = 0.15 ± 0.06 ‰; Δ^{204}Hg = -0.22 ± 0.17 ‰, all 1σ, n = 12), similar to

205   PDM cloud water and rainfall (Figure 3) and similar to global rainfall (Δ^{199}Hg = 0.35 ± 0.19 ‰; Δ^{200}Hg = 0.14

206   ± 0.06 ‰; Δ^{201}Hg = 0.35 ± 0.20 ‰ (Kwon et al., 2020). Demers et al. (2013) were the first to point out a negative

207   correlation between $\Delta^{200}Hg$ and $\Delta^{204}Hg$ in rainfall (Demers et al., 2013). Our work at the PDM extends this

208   relationship to RM, cloud water, and GEM phases (Figure 3). The presence of even- and odd-MIF in RM

209   suggests that globally observed Hg MIF signatures in rainfall are inherited from RM. Equally important, the

210   isotopic composition of RM is in stark contrast with that of GEM (Figure 3), even though the only

211   transformation that separates the two forms of Hg is net oxidation. This corroborates the suggestion that net

212   photochemical oxidation of GEM is responsible for even MIF (Chen et al., 2012), but it does not identify the

213   oxidative or reductive nature of the MIF inducing step among the myriad of possible reactions that drive

214   atmospheric net GEM oxidation.

215   Cloud water and rainfall $\delta^{202}Hg$ (0.17 ± 0.34 ‰) and $\Delta^{199}Hg$ (0.21 ± 0.04 ‰) show significant enrichment

216   in the heavier and in the odd Hg isotopes relative to mean RM $\delta^{202}Hg$ (-0.73 ± 0.63 ‰) and $\Delta^{199}Hg$ (0.44 ±

217   0.18 ‰)(both p<0.001, all mean, 1σ). We investigated if this is caused by in-cloud Hg^{II} photoreduction, by

218   incubating a rainfall sample spiked with 103 ng L^{-1} of NIST 3133 Hg. After 24h exposure to artificial sunlight

219   from a Xe lamp, the Hg concentration had dropped to 78 ng L^{-1} and small positive shifts in $\delta^{202}Hg$ (0.15 ‰),

220     $\Delta^{199}Hg$ (0.10‰), and $\Delta^{201}Hg$ (0.11‰), but not $\Delta^{200}Hg$ (-0.03‰) were detected. These observations are

221   consistent with limited, slow in-cloud Hg^{II} photoreduction affecting cloud water and rainfall MDF and odd-MIF.

222   Finally, we observe for the first time the $\Delta^{196}Hg$ signature to be near-zero (-0.06 ± 0.19‰, 2σ, n=2) in the 'GET

223   rain 6' sample (Figure 4), which has pronounced $\Delta^{199}Hg$ (0.70‰), $\Delta^{200}Hg$ (0.25‰), $\Delta^{201}Hg$ (0.82‰), and $\Delta^{204}Hg$

224   (-0.45‰). The observation that the least abundant ^{196}Hg, and most abundant ^{202}Hg isotope, both referenced to

225   ^{198}Hg, show near-zero MIF, further suggests that nuclear self-shielding is unlikely to be the mechanism

226   responsible for atmospheric Hg MIF.

227

228 $\delta^{202}Hg$ and $\Delta^{199}Hg$ variation during the high GOM event

229   We obtained additional evidence for odd and even MIF during net GEM oxidation from the high frequency (12-

230   24h) GEM isotope observations during the free tropospheric air mass intrusion, enriched in GOM and depleted

231   in GEM (Figure 1, days 4-6). The high GOM event showed GOM* concentrations of 252 pg m^{-3} from 23-24

232   Dec (48h mean). The GOM event was accompanied by low CO concentrations, depleted GEM concentrations,

233   and low relative humidity (Figure 1,2), which is consistent with previous studies and indicative of GOM

234   production by oxidation of GEM in a free tropospheric air mass (Gratz et al., 2015; Shah et al., 2016). Seven-

235   day back-trajectories of the GOM event and of the pre- (days 1-3) and post-event (days 7-9) air masses illustrate

236   the important control of cloudiness along the trajectory on detected GOM levels at the PDM (Figure 2). Pre/post-

237 GOM-event air masses generally travelled at 700-1000 hPa (3000m – 0m asl) over the N-Atlantic Ocean (35-

238 50°N) with RH from 60-100% and daytime solar radiation <200 w m^{-2} suggestive of GOM scavenging by clouds

239 (Figure 1,2). GOM-event air masses also travelled over the subtropical N-Atlantic Ocean, though at lower

240 latitudes (20-35°N), and higher altitudes of 500-900 hPa (5500m – 1500m asl) with RH from 0-40% and daytime

241 solar radiation from 200-500 w m^{-2} suggestive of clear skies. GOM-event mean ozone (47 ± 2 ppbv, sd), CO

242 (83 ± 3 ppbv, sd) and relative humidity ($34 \pm 10\%$, sd) are typical of lower to middle free tropospheric air. Both

243 the back trajectories and ozone, CO, RH characteristics suggest a negligible influence of stratospheric air on the

244 observed GOM-event.

245   A negative correlation between GEM and GOM* was observed during the 8-day study period of Dec 2012

246 with GOM*/GEM slope of -0.44 ± 0.10 ($r^2 = 0.66$; Figure 5). It has been previously suggested that GOM/GEM

247 slopes higher than -1 reflect the loss of newly produced GOM by scavenging processes, or the mixing with other

248 air masses with different GEM levels (Lyman and Jaffe, 2011; Swartzendruber et al., 2006). PBM concentrations

249 during the high-GOM event are uniformly low (mean, 4 pg m^{-3}) and RH and solar radiation levels along the

250 back trajectories do not support an important scavenging sink (Figure 2). A prerequisite for the GOM*/GEM

251 slope analysis is that the ensemble of observations has a common air mass origin, which is not the case here.

252 The back trajectory analysis of our 8-day observations suggests overlapping altitudes for pre- and post-event

253 (3000m – 0m asl) and GOM-event (5500m – 1500m asl) air masses. Published reviews of GEM altitude profiles

254 suggest little variation up to 5km (Holmes et al., 2010). However, observed and modeled boundary layer GEM

255 levels suggest maximum levels between 30-60°N, corresponding to mid-latitude emission sources, and declining

256 levels from 30°N to the equator (1% decrease in GEM per degree latitude, Holmes et al., 2010). As mentioned

257 above pre/post-event and GOM-event back trajectories point out different latitudinal origins of 20-35°N and 35-

258 50°N respectively. It seems therefore plausible that the original GEM levels in pre/post-event and GOM-event

259 levels air masses were different due to different latitudinal air mass origins. A correction for latitudinal

260 confounding allows estimating original GEM levels to be 15% lower in the GOM-event air masses, based on

261 the 1% drop in GEM per degree latitude, and yields a corrected GOM*/GEM slope of -0.88 (Figure 5, gray

262 line). The corrected slope is close to -1 and therefore suggests that all nearly GOM produced has been retained

263 within the free tropospheric air masses observed during the high GOM-event at the PDM.

264      $\delta^{202}Hg_{GEM}$ and $\Delta^{204}Hg_{GEM}$ during the high-GOM event were slightly but significantly higher, and $\Delta^{199}Hg_{GEM}$,

265 $\Delta^{200}Hg_{GEM}$ and $\Delta^{201}Hg_{GEM}$ slightly but significantly lower than pre- and post-event samples during 20 - 28 Dec

266 2012 (Figure 1; t-test all p<0.05). All five GEM isotope signatures are significantly correlated with GEM (Figure

267 6) and GOM concentration. Net GEM oxidation therefore seems to have caused significant MDF, odd-MIF and

268 even-MIF. The above analysis of the GOM event at the PDM suggests that the observed air masses represent

269 the reactants, products and isotope fractionation characteristics of net GEM oxidation. Because the GOM-event

270 was long-lived, displaying elevated GOM levels over 48 hours, we suggest that the GEM and GOM

271 concentration, and GEM isotope observations represent a snapshot of net GEM oxidation that has been little

272 influenced by further mixing with boundary layer air. This implies that the observed MDF, odd-MIF and even-

273 MIF has accompanied net GEM oxidation in the lower troposphere. Previous observations on even-MIF in

274 precipitation (Δ^{200}Hg only; Δ^{204}Hg not observed; Chen et al. 2012) led to the suggestion that even-MIF

275 originates at the tropopause or stratosphere. Our results suggest that the even-MIF mechanism also operates

276 within the free troposphere.

277   In Figure 6 we plot the GEM and RM (~GOM) isotope observations in Rayleigh diagrams, and fit MDF,

278 odd-MIF and even-MIF factors for net GEM oxidation. Assuming pre-/post GOM event isotope observations

279 as the starting point for GEM reactant in the free troposphere, we applied Rayleigh distillation equations for

280 residual δ^{202}Hg$_{GEM}$, Δ^{199}Hg$_{GEM}$, Δ^{200}Hg$_{GEM}$, Δ^{201}Hg$_{GEM}$, and Δ^{204}Hg$_{GEM}$ and for cumulative product GOM to

281 estimate corresponding isotope fractionation factors $\varepsilon^{202/198}_{MDF(GOM-GEM)}$ of -1.1±0.2‰, $\varepsilon^{199/198}_{MIF(GOM-GEM)}$ of

282 0.65±0.11‰, $\varepsilon^{200/198}_{MIF(GOM-GEM)}$ of 0.22±0.05‰, $\varepsilon^{201/198}_{MIF(GOM-GEM)}$ of 0.65±0.10‰, and $\varepsilon^{204/198}_{MIF(GOM-GEM)}$ of -0.39±0.12‰

283 for the net GEM to GOM conversion observed (Figure 6). It should be kept in mind that these fractionation

284 factor do not inform on whether oxidation or reduction is the underlying cause, i.e. they represent net oxidation.

285

286 **Atmospheric GEM and RM pool size**

287 GEM and RM represent the two dominant reduced and oxidized atmospheric Hg pools. The relative size of

288 these two pools is not very well constrained due to limited mountain-top and in-flight measurements and bias

289 in denuder based RM measurements (Jaffe et al., 2014). Recent global Hg chemistry and transport models

290 indicate that RM (500 Mg) represents 12% and GEM 88% (3600 Mg) of atmospheric Hg, most of this residing

291 in the free troposphere (Horowitz et al., 2017). Based on the newly observed free tropospheric RM and GEM

292 isotope compositions (this study), and previously observed rainfall Hg, and modeled Hg emission fluxes and

293 isotopic composition, we can estimate by isotopic mass balance the proportions of RM and GEM (Table 1). The

294 Δ^{200}Hg signature, is best suited for this, since it is not confounded by additional even-MIF in cloud water, ocean

295 or soil environment. Annual mean GEM Δ^{200}Hg at the PDM of -0.03±0.03‰ (Fu et al., 2016b) is identical to

296   GEM Δ^{200}Hg of -0.04‰ of the pre-/post GOM intrusion air masses, representing the northern hemisphere free

297   tropospheric GEM pool. RM Δ^{200}Hg at PDM (0.15‰) is similar to mean northern hemispheric rainfall Δ^{200}Hg

298   (0.13±0.06‰), suggesting that both values represent the free tropospheric RM pool. We use a model estimate

299   for Δ^{200}Hg (0.02±0.02‰) of global Hg emissions (Sun et al., 2019) to constrain the mass balance, and calculate

300   that 30±17% (1σ) of free tropospheric Hg should be present as RM in order to explain the rainfall, RM and

301   GEM Δ^{200}Hg observations. This would suggest that current RM observations and models underestimate the size

302   of the atmospheric RM pool by a factor of two. Our assessment is potentially biased due to the lack of

303   observations in the southern hemisphere.

304

312

313   **Author contributions**

314   J.E.S conceived the study. X.F, N.M., Y.X, M.J. and J.E.S performed field sampling. X.F, N.M., Y.X, M.J, LEHB,

315   JC. and J.E.S performed laboratory measurements. F.G. managed ancillary data collection at the PDM. X.F and

316   J.E.S wrote the draft manuscript, which was improved by contributions from all authors.

317

318   **Additional information**

319   All Hg stable isotope data measured and discussed in this study is reported in the Supplementary Data.

320

References

Amos, H. M., Jacob, D. J., Holmes, C. D., Fisher, J. A., Wang, Q., Yantosca, R. M., Corbitt, E. S., Galarneau, E., Rutter, A. P., Gustin, M. S., Steffen, A., Schauer, J. J., Graydon, J. A., St Louis, V. L., Talbot, R. W., Edgerton, E. S., Zhang, Y. and Sunderland, E. M.: Gas-particle partitioning of atmospheric Hg(II) and its effect on global mercury deposition, Atmospheric Chemistry and Physics, 12(1), 591–603, doi:10.5194/acp-12-591-2012, 2012.

Ariya, P. A., Amyot, M., Dastoor, A., Deeds, D., Feinberg, A., Kos, G., Poulain, A., Ryjkov, A., Semeniuk, K., Subir, M. and Toyota, K.: Mercury Physicochemical and Biogeochemical Transformation in the Atmosphere and at Atmospheric Interfaces: A Review and Future Directions, Chemical Reviews, 115(10), 3760–3802, doi:10.1021/cr500667e, 2015.

Bagnato, E., Tamburello, G., Avard, G., Martinez-Cruz, M., Enrico, M., Fu, X., Sprovieri, M. and Sonke, J. E.: Mercury fluxes from volcanic and geothermal sources: an update., Geological Society, London, Special Publications, doi 10.1144/SP410.2, 2014.

Berg, T., Pfaffhuber, K. A., Cole, A. S., Engelsen, O. and Steffen, A.: Ten-year trends in atmospheric mercury concentrations, meteorological effects and climate variables at Zeppelin, Ny-Ålesund, Atmospheric Chemistry and Physics, 13(13), 6575–6586, doi:10.5194/acp-13-6575-2013, 2013.

Bergquist, B. A. and Blum, J. D.: Mass-Dependent and -Independent Fractionation of Hg Isotopes by Photoreduction in Aquatic Systems., Science, 318, 417–420, 2007.

Blum, J. D. and Bergquist, B. A.: Reporting of variations in the natural isotopic composition of mercury., Analytical and Bioanalytical Chemistry, 388, 353–359, 2007.

Blum, J. D., Sherman, L. S. and Johnson, M. W.: Mercury Isotopes in Earth and Environmental Sciences, in Annual Review of Earth and Planetary Sciences, Vol 42, vol. 42, edited by R. Jeanloz, pp. 249–269., 2014.

Buchachenko, A. L., Ivanov, V. L., Roznyatovskii, V. A., Artamkina, G. A., Vorob'ev, A. K. and Ustynyuk, Y. A.: Magnetic isotope effect for mercury nuclei in photolysis of Bis(p-trifluoromethylbenzyl)mercury., Doklady Physical Chemistry, 413, 39–41, 2007.

Chen, J., Hintelmann, H., Feng, X. and Dimock, B.: Unusual fractionation of both odd and even mercury isotopes in precipitation from Peterborough, ON, Canada, Geochimica et Cosmochimica Acta, 90, 33–46, doi:10.1016/j.gca.2012.05.005, 2012.

Demers, J. D., Blum, J. D. and Zak, D. R.: Mercury isotopes in a forested ecosystem: Implications for air-surface exchange dynamics and the global mercury cycle, Global Biogeochemical Cycles, 27(1), 222–238, doi:10.1002/gbc.20021, 2013.

Demoz, B., Collett, J., J. L. and Daube, J., B. C.: On the Caltech Active Strand Cloudwater Collectors., Atmospheric Research, 41, 47–62, 1996.

Dibble, T. S., Tetu, H. L., Jiao, Y., Thackray, C. P. and Jacob, D. J.: Modeling the OH-Initiated Oxidation of Mercury in the Global Atmosphere without Violating Physical Laws, Journal of Physical Chemistry A, 124(2), 444–453, doi:10.1021/acs.jpca.9b10121, 2020.

356 Donohoue, D. L., Bauer, D., Cossairt, B. and Hynes, A.: Temperature and pressure dependent rate coefficients for the
357 reaction of Hg with Br and the reaction of Br with Br: A pulsed laser photolysis-pulsed laser induced fluorescence
358 study, Journal of Physical Chemistry A, 110, 6623–6632, 2006.

359 Enrico, M., Le Roux, G., Maruszczak, N., Heimbürger, L.-E., Claustres, A., Fu, X., Sun, R. and Sonke, J. E.:
360 Atmospheric mercury transfer to peat bogs dominated by gaseous elemental mercury dry deposition., Environmental
361 Science & Technology, doi:10.1021/acs.est.5b06058, 2016.

362 Fitzgerald, W. F. and Lamborg, C. H.: Geochemistry of Mercury in the Environment, in Treatise on Geochemistry,
363 vol. 9, edited by E. D. Holland and K. K. Turekian, pp. 107–148, Elsevier-Pergamon, Oxford., 2004.

364 Fu, X., Heimburger, L. E. and Sonke, J. E.: Collection of atmospheric gaseous mercury for stable isotope analysis
365 using iodine- and chlorine-impregnated activated carbon traps, Journal of Analytical Atomic Spectrometry, DOI:
366 10.1039/C3JA50356A, 2014.

367 Fu, X. W., Maruszczak, N., Heimbürger, L. E., Sauvage, B., Gheusi, F. and Sonke, J. E.: Atmospheric mercury
368 speciation dynamics at the high-altitude Pic du Midi Observatory, southern France, Atmospheric Chemistry and
369 Physics, 16, 5623–5639, doi:10.5194/acp-16-5623-2016, 2016a.

370 Fu, X. W., Maruszczak, N., Wang, X., Gheusi, F. and Sonke, J. E.: The isotopic composition of total gaseous mercury
371 in the free troposphere of the Pic du Midi Observatory (2877 m a.s.l, France), Environmental Science & Technology,
372 submitted, 2016b.

373 Gheusi, F., Ravetta, F., Delbarre, H., Tsamalis, C., Chevalier-Rosso, A., Leroy, C., Augustin, P., Delmas, R., Ancellet,
374 G., Athier, G., Bouchou, P., Campistron, B., Cousin, J. M., Fourmentin, M. and Meyerfeld, Y.: Pic 2005, a field
375 campaign to investigate low-tropospheric ozone variability in the Pyrenees, Atmospheric Research, 101(3), 640–665,
376 doi:10.1016/j.atmosres.2011.04.014, 2011.

377 Gratz, L., Keeler, G., Blum, J. and Sherman, L. S.: Isotopic composition and fractionation of mercury in Great Lakes
378 precipitation and ambient air, Environmental Science and Technology, 44, 7764–7770, 2010.

379 Gratz, L. E., Ambrose, J. L., Jaffe, D. A., Shah, V., Jaegle, L., Stutz, J., Festa, J., Spolaor, M., Tsai, C., Selin, N. E.,
380 Song, S., Zhou, X., Weinheimer, A. J., Knapp, D. J., Montzka, D. D., Flocke, F. M., Campos, T. L., Apel, E.,
381 Hornbrook, R., Blake, N. J., Hall, S., Tyndall, G. S., Reeves, M., Stechman, D. and Stell, M.: Oxidation of mercury
382 by bromine in the subtropical Pacific free troposphere, Geophysical Research Letters, 42(23),
383 doi:10.1002/2015gl066645, 2015.

384 Grissom, C. B.: Magnetic field effects in biology: A survey of possible mechanisms with emphasis on radical-pair
385 recombination, Chemical Reviews, 95, 3–24, 1995.

386 Holmes, C. D., Jacob, D. J., Corbitt, E. S., Mao, J., Yang, X., Talbot, R. and Slemr, F.: Global atmospheric model for
387 mercury including oxidation by bromine atoms, Atmospheric Chemistry and Physics, 10, 12037–12057, 2010.

388 Horowitz, H. M., Jacob, D. J., Zhang, Y., Dibble, T. S., Slemr, F., Amos, H. M., Schmidt, J. A., Corbitt, E. S., Marais,
389 E. A. and Sunderland, E. M.: A new mechanism for atmospheric mercury redox chemistry: implications for the global
390 mercury budget, Atmospheric Chemistry and Physics, 17(10), 6353–6371, doi:10.5194/acp-17-6353-2017, 2017.

391 Hulin, M., Gheusi, F., Lothon, M., Pont, V., Lohou, F., Ramonet, M., Delmotte, M., Derrien, S., Athier, G., Meyerfeld,
392 Y., Bezombes, Y., Augustin, P. and Ravetta, F.: Observations of Thermally Driven Circulations in the Pyrenees:
393 Comparison of Detection Methods and Impact on Atmospheric Composition Measured at a Mountaintop, Journal of
394 Applied Meteorology and Climatology, 58(4), 717–740, doi:10.1175/JAMC-D-17-0268.1, 2019.

395 Jaffe, D. A., Lyman, S., Amos, H. M., Gustin, M. S., Huang, J., Selin, N. E., Levin, L., ter Schure, A., Mason, R. P.,
396 Talbot, R., Rutter, A., Finley, B., Jaegle, L., Shah, V., McClure, C., Arnbrose, J., Gratz, L., Lindberg, S., Weiss-
397 Penzias, P., Sheu, G.-R., Feddersen, D., Horvat, M., Dastoor, A., Hynes, A. J., Mao, H., Sonke, J. E., Slemr, F., Fisher,
398 J. A., Ebinghaus, R., Zhang, Y. and Edwards, G.: Progress on Understanding Atmospheric Mercury Hampered by
399 Uncertain Measurements, Environmental Science & Technology, 48(13), 7204–7206, doi:10.1021/es5026432, 2014.

400 Jiskra, M., Wiederhold, J. G., Skyllberg, U., Kronberg, R.-M., Hajdas, I. and Kretzschmar, R.: Mercury Deposition
401 and Re-emission Pathways in Boreal Forest Soils Investigated with Hg Isotope Signatures, Environmental Science
402 & Technology, 49(12), 7188–7196, doi:10.1021/acs.est.5b00742, 2015.

403 Jiskra, M., Sonke, J. E., Agnan, Y., Helmig, D. and Obrist, D.: Insights from mercury stable isotopes on terrestrial-
404 atmosphere exchange of Hg(0) in the Arctic tundra, Biogeosciences, 16(20), 4051–4064, doi:10.5194/bg-16-4051-
405 2019, 2019.

406 Kritee, K., Blum, J. D., Reinfelder, J. R. and Barkay, T.: Microbial stable isotope fractionation of mercury: A synthesis
407 of present understanding and future directions, Chemical Geology, this issue, doi:10.1016/j.chemgeo.2012.08.017,
408 2012.

409 Kwon, S. Y., Blum, J. D., Yin, R., Tsui, M. T.-K., Yang, Y. H. and Choi, J. W.: Mercury stable isotopes for monitoring
410 the effectiveness of the Minamata Convention on Mercury, Earth-Science Reviews, 203, 103111,
411 doi:https://doi.org/10.1016/j.earscirev.2020.103111, 2020.

412 Lyman, S. N. and Jaffe, D. A.: Formation and fate of oxidized mercury in the upper troposphere and lower
413 stratosphere, Nature Geoscience, 5(2), 114–117, doi:10.1038/ngeo1353, 2011.

414 Lynam, M. M. and Keeler, G. J.: Comparison of methods for particulate phase mercury analysis: sampling and
415 analysis, Analytical and Bioanalytical Chemistry, 374(6), 1009–1014, doi:10.1007/s00216-002-1584-4, 2002.

416 Marusczak, N., Sonke, J. E., Fu, X. and Jiskra, M.: Tropospheric GOM at the Pic du Midi Observatory-Correcting
417 Bias in Denuder Based Observations, Environmental Science & Technology, 51(2), 863–869,
418 doi:10.1021/acs.est.6b04999, 2017.

419 Motta, L. C., Blum, J. D., Johnson, M. W., Umhau, B. P., Popp, B. N., Washburn, S. J., Drazen, J. C., Benitez-Nelson,
420 C. R., Hannides, C. C. S., Close, H. G. and Lamborg, C. H.: Mercury Cycling in the North Pacific Subtropical Gyre
421 as Revealed by Mercury Stable Isotope Ratios, Global Biogeochemical Cycles, 33(6), 777–794,
422 doi:10.1029/2018GB006057, 2019.

423 Motta, L. C., Kritee, K., Blum, J. D., Tsz-Ki Tsui, M. and Reinfelder, J. R.: Mercury Isotope Fractionation during the
424 Photochemical Reduction of Hg(II) Coordinated with Organic Ligands., The journal of physical chemistry. A,
425 doi:10.1021/acs.jpca.9b06308, 2020a.

426 Motta, L. C., Chien, A. D., Rask, A. E. and Zimmerman, P. M.: Mercury Magnetic Isotope Effect: A Plausible

427 Photochemical Mechanism, J. Phys. Chem. A, 124(19), 3711–3719, doi:10.1021/acs.jpca.0c00661, 2020b.

428 Obrist, D., Agnan, Y., Jiskra, M., Olson, C. L., Colegrove, D. P., Hueber, J., Moore, C. W., Sonke, J. E. and Helmig,
429 D.: Tundra uptake of atmospheric elemental mercury drives Arctic mercury pollution, Nature, 547(7662), 201-+,
430 doi:10.1038/nature22997, 2017.

431 Saiz-Lopez, A., Sitkiewicz, S. P., Roca-Sanjuán, D., Oliva-Enrich, J. M., Dávalos, J. Z., Notario, R., Jiskra, M., Xu,
432 Y., Wang, F., Thackray, C. P., Sunderland, E. M., Jacob, D. J., Travnikov, O., Cuevas, C. A., Acuña, A. U., Rivero,
433 D., Plane, J. M. C., Kinnison, D. E. and Sonke, J. E.: Photoreduction of gaseous oxidized mercury changes global
434 atmospheric mercury speciation, transport and deposition, Nature Communications, 9(1), 4796, doi:10.1038/s41467-
435 018-07075-3, 2018.

436 Saiz-Lopez, A., Acuña, A. U., Trabelsi, T., Carmona-García, J., Dávalos, J. Z., Rivero, D., Cuevas, C. A., Kinnison,
437 D. E., Sitkiewicz, S. P., Roca-Sanjuán, D. and Francisco, J. S.: Gas-Phase Photolysis of Hg(I) Radical Species: A
438 New Atmospheric Mercury Reduction Process, J. Am. Chem. Soc., 141(22), 8698–8702, doi:10.1021/jacs.9b02890,
439 2019.

440 Schauble, E. A.: Role of nuclear volume in driving equilibrium isotope fractionation of mercury, thallium, and other
441 very heavy elements., Geochimica et Cosmochimca Acta, 71, 2170–2189, 2007.

442 Seigneur, C. and Lohman, K.: Effect of bromine chemistry on the atmospheric mercury cycle, Journal of Geophysical
443 Research - Atmosphere, 113, D23309, 2008.

444 Seigneur, C., Vijayaraghavan, K., Lohman, K., Karamchandani, P. and Scott, C.: Global Source Attribution for
445 Mercury Deposition in the United States, Environmental Science and Technology, 38, 555–569, 2004.

446 Shah, V., Jaegle, L., Gratz, L. E., Ambrose, J. L., Jaffe, D. A., Selin, N. E., Song, S., Campos, T. L., Flocke, F. M.,
447 Reeves, M., Stechman, D., Stell, M., Festa, J., Stutz, J., Weinheimer, A. J., Knapp, D. J., Montzka, D. D., Tyndall, G.
448 S., Apel, E. C., Hornbrook, R. S., Hills, A. J., Riemer, D. D., Blake, N. J., Cantrell, C. A. and Mauldin, R. L.: Origin
449 of oxidized mercury in the summertime free troposphere over the southeastern US, Atmospheric Chemistry and
450 Physics, 16(3), 1511–1530, doi:10.5194/acp-16-1511-2016, 2016.

451 Sherman, L. S., Blum, J. D., Keeler, G. J., Demers, J. D. and Dvonch, J. T.: Investigation of Local Mercury Deposition
452 from a Coal-Fired Power Plant Using Mercury Isotopes, Environmental Science & Technology, 46(1), 382–390,
453 doi:10.1021/es202793c, 2012.

454 Steffen, A., Schroeder, W., Macdonald, R., Poissant, L. and Konoplev, A.: Mercury in the Arctic atmosphere: An
455 analysis of eight years of measurements of GEM at Alert (Canada) and a comparison with observations at Amderma
456 (Russia) and Kuujjuarapik (Canada), Science of the Total Environment, 342(1–3), 185–198,
457 doi:10.1016/j.scitotenv.2004.12.048, 2005.

458 Streets, D. G., Horowitz, H. M., Lu, Z., Levin, L., Thackray, C. P. and Sunderland, E. M.: Global and regional trends
459 in mercury emissions and concentrations, 2010-2015, Atmospheric Environment, 201, 417–427,
460 doi:10.1016/j.atmosenv.2018.12.031, 2019.

461 Sun, G., Sommar, J., Feng, X., Lin, C.-J., Ge, M., Wang, W., Yin, R., Fu, X. and Shang, L.: Mass-Dependent and -
462 Independent Fractionation of Mercury Isotope during Gas-Phase Oxidation of Elemental Mercury Vapor by Atomic

463   Cl and Br, Environ. Sci. Technol., 50(17), 9232–9241, doi:10.1021/acs.est.6b01668, 2016.

464   Sun, R., Enrico, M., Heimbürger, L.-E., Scott, C. and Sonke, J. E.: A double-stage tube furnace-acid-trapping protocol
465   for the pre-concentration of mercury from solid samples for isotopic analysis, Analytical and Bioanalytical Chemistry,
466   405(21), 6771–6781, doi:10.1007/s00216-013-7152-2, 2013.

467   Sun, R., Jiskra, M., Amos, H. M., Zhang, Y., Sunderland, E. M. and Sonke, J. E.: Modelling the mercury stable isotope
468   distribution of Earth surface reservoirs: Implications for global Hg cycling, Geochimica et Cosmochimica Acta, 246,
469   156–173, doi:https://doi.org/10.1016/j.gca.2018.11.036, 2019.

470   Swartzendruber, P. C., Jaffe, J. A., Prestbo, E. M., Weiss-Penzias, P., Selin, N. E., Park, R., Jacob, D. J., Strode, S.
471   and Jaegle, L.: Observations of reactive gaseous mercury in the free troposphere at the Mount Bachelor Observatory,
472   Journal of Geophysical Research, 111, D24301, 2006.

473   Timonen, H., Ambrose, J. L. and Jaffe, D. A.: Oxidation of elemental Hg in anthropogenic and marine airmasses,
474   Atmospheric Chemistry and Physics, 13(5), 2827–2836, doi:10.5194/acp-13-2827-2013, 2013.

475   Turro, N. J.: Influence of nuclear spin on chemical, reactions: Magnetic isotope and.magnetic field effects (A Review),
476   Proceedings of the National Academy of Science USA, 80, 609–621, 1983.

477   Wang, F., Saiz-Lopez, A., Mahajan, A. S., Gomez Martin, J. C., Armstrong, D., Lemes, M., Hay, T. and Prados-
478   Roman, C.: Enhanced production of oxidised mercury over the tropical Pacific Ocean: a key missing oxidation
479   pathway, Atmospheric Chemistry and Physics, 14(3), 1323–1335, doi:10.5194/acp-14-1323-2014, 2014.

480   Wang, Z., Chen, J., Feng, X., Hintelmann, H., Yuan, S., Cai, H., Huang, Q., Wang, S. and Wang, F.: Mass-dependent
481   and mass-independent fractionation of mercury isotopes in precipitation from Guiyang, SW China, Comptes Rendus
482   Geoscience, 347(7), 358–367, doi:https://doi.org/10.1016/j.crte.2015.02.006, 2015.

483   Weiss-Penzias, P., Amos, H. M., Selin, N. E., Gustin, M. S., Jaffe, D. A., Obrist, D., Sheu, G. R. and Giang, A.: Use
484   of a global model to understand speciated atmospheric mercury observations at five high-elevation sites, Atmospheric
485   Chemistry and Physics, 15(3), 1161–1173, doi:10.5194/acp-15-1161-2015, 2015.

486   Wiederhold, J. G., Cramer, C. J., Daniel, K., Infante, I., Bourdon, B. and Kretzschmar, R.: Equilibrium mercury
487   isotope fractionation between dissolved Hg(II) species and thiol-bound Hg, Environmental Science and Technology,
488   44, 4191–4197, 2010.

489   Yang, X., Jiskra, M. and Sonke, J. E.: Experimental rainwater divalent mercury speciation and photoreduction rates
490   in the presence of halides and organic carbon, Science of The Total Environment, 697, 133821,
491   doi:https://doi.org/10.1016/j.scitotenv.2019.133821, 2019.

492   Zheng, W. and Hintelmann, H.: Mercury isotope fractionation during photoreduction in natural water is controlled
493   by its Hg/DOC ratio., Geochimica et Cosmochimca Acta, 73, 6704–6715, 2009.

494   Zheng, W. and Hintelmann, H.: Isotope Fractionation of Mercury during Its Photochemical Reduction by Low-
495   Molecular-Weight Organic Compounds, Journal of Physical Chemistry A, 114, 4246–4253, 2010.

496

Ariya, P. A., Amyot, M., Dastoor, A., Deeds, D., Feinberg, A., Kos, G., Poulain, A., Ryjkov, A., Semeniuk, K., Subir, M. and Toyota, K.: Mercury Physicochemical and Biogeochemical Transformation in the Atmosphere and at Atmospheric Interfaces: A Review and Future Directions, Chemical Reviews, 115(10), 3760–3802, doi:10.1021/cr500667e, 2015.

Bagnato, E., Tamburello, G., Avard, G., Martinez-Cruz, M., Enrico, M., Fu, X., Sprovieri, M. and Sonke, J. E.: Mercury fluxes from volcanic and geothermal sources: an update., Geological Society, London, Special Publications, doi 10.1144/SP410.2, 2014.

Berg, T., Pfaffhuber, K. A., Cole, A. S., Engelsen, O. and Steffen, A.: Ten-year trends in atmospheric mercury concentrations, meteorological effects and climate variables at Zeppelin, Ny-Ålesund, Atmospheric Chemistry and Physics, 13(13), 6575–6586, doi:10.5194/acp-13-6575-2013, 2013.

Bergquist, B. A. and Blum, J. D.: Mass-Dependent and -Independent Fractionation of Hg Isotopes by Photoreduction in Aquatic Systems., Science, 318, 417–420, 2007.

Blum, J. D. and Bergquist, B. A.: Reporting of variations in the natural isotopic composition of mercury., Analytical and Bioanalytical Chemistry, 388, 353–359, 2007.

Blum, J. D., Sherman, L. S. and Johnson, M. W.: Mercury Isotopes in Earth and Environmental Sciences, in Annual Review of Earth and Planetary Sciences, Vol 42, vol. 42, edited by R. Jeanloz, pp. 249–269., 2014.

Buchachenko, A. L., Ivanov, V. L., Roznyatovskii, V. A., Artamkina, G. A., Vorob'ev, A. K. and Ustynyuk, Y. A.: Magnetic isotope effect for mercury nuclei in photolysis of Bis(p-trifluoromethylbenzyl)mercury., Doklady Physical Chemistry, 413, 39–41, 2007.

Chen, J., Hintelmann, H., Feng, X. and Dimock, B.: Unusual fractionation of both odd and even mercury isotopes in precipitation from Peterborough, ON, Canada, Geochimica et Cosmochimica Acta, 90, 33–46, doi:10.1016/j.gca.2012.05.005, 2012.

Demers, J. D., Blum, J. D. and Zak, D. R.: Mercury isotopes in a forested ecosystem: Implications for air-surface exchange dynamics and the global mercury cycle, Global Biogeochemical Cycles, 27(1), 222–238, doi:10.1002/gbc.20021, 2013.

Demoz, B., Collett, J., J. L. and Daube, J., B. C.: On the Caltech Active Strand Cloudwater Collectors., Atmospheric Research, 41, 47–62, 1996.

Dibble, T. S., Tetu, H. L., Jiao, Y., Thackray, C. P. and Jacob, D. J.: Modeling the OH-Initiated Oxidation of Mercury in the Global Atmosphere without Violating Physical Laws, Journal of Physical Chemistry A, 124(2), 444–453, doi:10.1021/acs.jpca.9b10121, 2020.

Donohoue, D. L., Bauer, D., Cossairt, B. and Hynes, A.: Temperature and pressure dependent rate coefficients for the reaction of Hg with Br and the reaction of Br with Br: A pulsed laser photolysis-pulsed laser induced fluorescence study, Journal of Physical Chemistry A, 110, 6623–6632, 2006.

Enrico, M., Le Roux, G., Marusczak, N., Heimbürger, L.-E., Claustres, A., Fu, X., Sun, R. and Sonke, J. E.: Atmospheric mercury transfer to peat bogs dominated by gaseous elemental mercury dry deposition., Environmental

532   Science & Technology, doi:10.1021/acs.est.5b06058, 2016.

533   Fitzgerald, W. F. and Lamborg, C. H.: Geochemistry of Mercury in the Environment, in Treatise on Geochemistry,
534   vol. 9, edited by E. D. Holland and K. K. Turekian, pp. 107–148, Elsevier-Pergamon, Oxford., 2004.

535   Fu, X., Heimburger, L. E. and Sonke, J. E.: Collection of atmospheric gaseous mercury for stable isotope analysis
536   using iodine- and chlorine-impregnated activated carbon traps, Journal of Analytical Atomic Spectrometry, DOI:
537   10.1039/C3JA50356A, 2014.

538   Fu, X. W., Maruszak, N., Heimbürger, L. E., Sauvage, B., Gheusi, F. and Sonke, J. E.: Atmospheric mercury
539   speciation dynamics at the high-altitude Pic du Midi Observatory, southern France, Atmospheric Chemistry and
540   Physics, 16, 5623–5639, doi:10.5194/acp-16-5623-2016, 2016a.

541   Fu, X. W., Maruszak, N., Wang, X., Gheusi, F. and Sonke, J. E.: The isotopic composition of total gaseous mercury
542   in the free troposphere of the Pic du Midi Observatory (2877 m a.s.l, France), Environmental Science & Technology,
543   submitted, 2016b.

544   Gheusi, F., Ravetta, F., Delbarre, H., Tsamalis, C., Chevalier-Rosso, A., Leroy, C., Augustin, P., Delmas, R., Ancellet,
545   G., Athier, G., Bouchou, P., Campistron, B., Cousin, J. M., Fourmentin, M. and Meyerfeld, Y.: Pic 2005, a field
546   campaign to investigate low-tropospheric ozone variability in the Pyrenees, Atmospheric Research, 101(3), 640–665,
547   doi:10.1016/j.atmosres.2011.04.014, 2011.

548   Gratz, L., Keeler, G., Blum, J. and Sherman, L. S.: Isotopic composition and fractionation of mercury in Great Lakes
549   precipitation and ambient air, Environmental Science and Technology, 44, 7764–7770, 2010.

550   Gratz, L. E., Ambrose, J. L., Jaffe, D. A., Shah, V., Jaegle, L., Stutz, J., Festa, J., Spolaor, M., Tsai, C., Selin, N. E.,
551   Song, S., Zhou, X., Weinheimer, A. J., Knapp, D. J., Montzka, D. D., Flocke, F. M., Campos, T. L., Apel, E.,
552   Hornbrook, R., Blake, N. J., Hall, S., Tyndall, G. S., Reeves, M., Stechman, D. and Stell, M.: Oxidation of mercury
553   by bromine in the subtropical Pacific free troposphere, Geophysical Research Letters, 42(23),
554   doi:10.1002/2015gl066645, 2015.

555   Grissom, C. B.: Magnetic field effects in biology: A survey of possible mechanisms with emphasis on radical-pair
556   recombination, Chemical Reviews, 95, 3–24, 1995.

557   Holmes, C. D., Jacob, D. J., Corbitt, E. S., Mao, J., Yang, X., Talbot, R. and Slemr, F.: Global atmospheric model for
558   mercury including oxidation by bromine atoms, Atmospheric Chemistry and Physics, 10, 12037–12057, 2010.

559   Horowitz, H. M., Jacob, D. J., Zhang, Y., Dibble, T. S., Slemr, F., Amos, H. M., Schmidt, J. A., Corbitt, E. S., Marais,
560   E. A. and Sunderland, E. M.: A new mechanism for atmospheric mercury redox chemistry: implications for the global
561   mercury budget, Atmospheric Chemistry and Physics, 17(10), 6353–6371, doi:10.5194/acp-17-6353-2017, 2017.

562   Hulin, M., Gheusi, F., Lothon, M., Pont, V., Lohou, F., Ramonet, M., Delmotte, M., Derrien, S., Athier, G., Meyerfeld,
563   Y. : Observations of plain-mountain circulation in the Pyrenees : detection methods and impact on atmospheric
564   composition measured at a mountain top, J. Applied. Meteor. Climatol, 2019, 58, 717–740,
565   https://doi.org/10.1175/JAMC-D-17-0268.1.

566   Jaffe, D. A., Lyman, S., Amos, H. M., Gustin, M. S., Huang, J., Selin, N. E., Levin, L., ter Schure, A., Mason, R. P.,

Talbot, R., Rutter, A., Finley, B., Jaegle, L., Shah, V., McClure, C., Arnbrose, J., Gratz, L., Lindberg, S., Weiss-Penzias, P., Sheu, G.-R., Feddersen, D., Horvat, M., Dastoor, A., Hynes, A. J., Mao, H., Sonke, J. E., Slemr, F., Fisher, J. A., Ebinghaus, R., Zhang, Y. and Edwards, G.: Progress on Understanding Atmospheric Mercury Hampered by Uncertain Measurements, Environmental Science & Technology, 48(13), 7204–7206, doi:10.1021/es5026432, 2014.

Jiskra, M., Wiederhold, J. G., Skyllberg, U., Kronberg, R.-M., Hajdas, I. and Kretzschmar, R.: Mercury Deposition and Re-emission Pathways in Boreal Forest Soils Investigated with Hg Isotope Signatures, Environmental Science & Technology, 49(12), 7188–7196, doi:10.1021/acs.est.5b00742, 2015.

Jiskra, M., Sonke, J. E., Agnan, Y., Helmig, D. and Obrist, D.: Insights from mercury stable isotopes on terrestrial-atmosphere exchange of Hg(0) in the Arctic tundra, Biogeosciences, 16(20), 4051–4064, doi:10.5194/bg-16-4051-2019, 2019.

Kritee, K., Blum, J. D., Reinfelder, J. R. and Barkay, T.: Microbial stable isotope fractionation of mercury: A synthesis of present understanding and future directions, Chemical Geology, this issue, doi:10.1016/j.chemgeo.2012.08.017, 2012.

Kwon, S. Y., Blum, J. D., Yin, R., Tsui, M. T.-K., Yang, Y. H. and Choi, J. W.: Mercury stable isotopes for monitoring the effectiveness of the Minamata Convention on Mercury, Earth-Science Reviews, 203, 103111, doi:https://doi.org/10.1016/j.earscirev.2020.103111, 2020.

Lyman, S. N. and Jaffe, D. A.: Formation and fate of oxidized mercury in the upper troposphere and lower stratosphere, Nature Geoscience, 5(2), 114–117, doi:10.1038/ngeo1353, 2011.

Lynam, M. M. and Keeler, G. J.: Comparison of methods for particulate phase mercury analysis: sampling and analysis, Analytical and Bioanalytical Chemistry, 374(6), 1009–1014, doi:10.1007/s00216-002-1584-4, 2002.

Maruszczak, N., Sonke, J. E., Fu, X. and Jiskra, M.: Tropospheric GOM at the Pic du Midi Observatory-Correcting Bias in Denuder Based Observations, Environmental Science & Technology, 51(2), 863–869, doi:10.1021/acs.est.6b04999, 2017.

Motta, L. C., Blum, J. D., Johnson, M. W., Umhau, B. P., Popp, B. N., Washburn, S. J., Drazen, J. C., Benitez-Nelson, C. R., Hannides, C. C. S., Close, H. G. and Lamborg, C. H.: Mercury Cycling in the North Pacific Subtropical Gyre as Revealed by Mercury Stable Isotope Ratios, Global Biogeochemical Cycles, 33(6), 777–794, doi:10.1029/2018GB006057, 2019.

Motta, L. C., Kritee, K., Blum, J. D., Tsz-Ki Tsui, M. and Reinfelder, J. R.: Mercury Isotope Fractionation during the Photochemical Reduction of Hg(II) Coordinated with Organic Ligands., The journal of physical chemistry. A, doi:10.1021/acs.jpca.9b06308, 2020a.

Motta, L. C., Chien, A. D., Rask, A. E. and Zimmerman, P. M.: Mercury Magnetic Isotope Effect: A Plausible Photochemical Mechanism, J. Phys. Chem. A, 124(19), 3711–3719, doi:10.1021/acs.jpca.0c00661, 2020b.

Obrist, D., Agnan, Y., Jiskra, M., Olson, C. L., Colegrove, D. P., Hueber, J., Moore, C. W., Sonke, J. E. and Helmig, D.: Tundra uptake of atmospheric elemental mercury drives Arctic mercury pollution, Nature, 547(7662), 201-+, doi:10.1038/nature22997, 2017.

602 Saiz-Lopez, A., Sitkiewicz, S. P., Roca-Sanjuán, D., Oliva-Enrich, J. M., Dávalos, J. Z., Notario, R., Jiskra, M., Xu,
603 Y., Wang, F., Thackray, C. P., Sunderland, E. M., Jacob, D. J., Travnikov, O., Cuevas, C. A., Acuña, A. U., Rivero,
604 D., Plane, J. M. C., Kinnison, D. E. and Sonke, J. E.: Photoreduction of gaseous oxidized mercury changes global
605 atmospheric mercury speciation, transport and deposition, Nature Communications, 9(1), 4796, doi:10.1038/s41467-
606 018-07075-3, 2018.

607 Saiz-Lopez, A., Acuña, A. U., Trabelsi, T., Carmona-García, J., Dávalos, J. Z., Rivero, D., Cuevas, C. A., Kinnison,
608 D. E., Sitkiewicz, S. P., Roca-Sanjuán, D. and Francisco, J. S.: Gas-Phase Photolysis of Hg(I) Radical Species: A
609 New Atmospheric Mercury Reduction Process, J. Am. Chem. Soc., 141(22), 8698–8702, doi:10.1021/jacs.9b02890,
610 2019.

611 Schauble, E. A.: Role of nuclear volume in driving equilibrium isotope fractionation of mercury, thallium, and other
612 very heavy elements., Geochimica et Cosmochimca Acta, 71, 2170–2189, 2007.

613 Seigneur, C. and Lohman, K.: Effect of bromine chemistry on the atmospheric mercury cycle, Journal of Geophysical
614 Research - Atmosphere, 113, D23309, 2008.

615 Seigneur, C., Vijayaraghavan, K., Lohman, K., Karamchandani, P. and Scott, C.: Global Source Attribution for
616 Mercury Deposition in the United States, Environmental Science and Technology, 38, 555–569, 2004.

617 Shah, V., Jaegle, L., Gratz, L. E., Ambrose, J. L., Jaffe, D. A., Selin, N. E., Song, S., Campos, T. L., Flocke, F. M.,
618 Reeves, M., Stechman, D., Stell, M., Festa, J., Stutz, J., Weinheimer, A. J., Knapp, D. J., Montzka, D. D., Tyndall, G.
619 S., Apel, E. C., Hornbrook, R. S., Hills, A. J., Riemer, D. D., Blake, N. J., Cantrell, C. A. and Mauldin, R. L.: Origin
620 of oxidized mercury in the summertime free troposphere over the southeastern US, Atmospheric Chemistry and
621 Physics, 16(3), 1511–1530, doi:10.5194/acp-16-1511-2016, 2016.

622 Sherman, L. S., Blum, J. D., Keeler, G. J., Demers, J. D. and Dvonch, J. T.: Investigation of Local Mercury Deposition
623 from a Coal-Fired Power Plant Using Mercury Isotopes, Environmental Science & Technology, 46(1), 382–390,
624 doi:10.1021/es202793c, 2012.

625 Steffen, A., Schroeder, W., Macdonald, R., Poissant, L. and Konoplev, A.: Mercury in the Arctic atmosphere: An
626 analysis of eight years of measurements of GEM at Alert (Canada) and a comparison with observations at Amderma
627 (Russia) and Kuujjuarapik (Canada), Science of the Total Environment, 342(1–3), 185–198,
628 doi:10.1016/j.scitotenv.2004.12.048, 2005.

629 Streets, D. G., Horowitz, H. M., Lu, Z., Levin, L., Thackray, C. P. and Sunderland, E. M.: Global and regional trends
630 in mercury emissions and concentrations, 2010-2015, Atmospheric Environment, 201, 417–427,
631 doi:10.1016/j.atmosenv.2018.12.031, 2019.

632 Sun, G., Sommar, J., Feng, X., Lin, C.-J., Ge, M., Wang, W., Yin, R., Fu, X. and Shang, L.: Mass-Dependent and -
633 Independent Fractionation of Mercury Isotope during Gas-Phase Oxidation of Elemental Mercury Vapor by Atomic
634 Cl and Br, Environ. Sci. Technol., 50(17), 9232–9241, doi:10.1021/acs.est.6b01668, 2016.

635 Sun, R., Enrico, M., Heimbürger, L.-E., Scott, C. and Sonke, J. E.: A double-stage tube furnace-acid-trapping protocol
636 for the pre-concentration of mercury from solid samples for isotopic analysis, Analytical and Bioanalytical Chemistry,
637 405(21), 6771–6781, doi:10.1007/s00216-013-7152-2, 2013.

638   Sun, R., Jiskra, M., Amos, H. M., Zhang, Y., Sunderland, E. M. and Sonke, J. E.: Modelling the mercury stable isotope
639   distribution of Earth surface reservoirs: Implications for global Hg cycling, Geochimica et Cosmochimica Acta, 246,
640   156–173, doi:https://doi.org/10.1016/j.gca.2018.11.036, 2019.

641   Swartzendruber, P. C., Jaffe, J. A., Prestbo, E. M., Weiss-Penzias, P., Selin, N. E., Park, R., Jacob, D. J., Strode, S.
642   and Jaegle, L.: Observations of reactive gaseous mercury in the free troposphere at the Mount Bachelor Observatory,
643   Journal of Geophysical Research, 111, D24301, 2006.

644   Timonen, H., Ambrose, J. L. and Jaffe, D. A.: Oxidation of elemental Hg in anthropogenic and marine airmasses,
645   Atmospheric Chemistry and Physics, 13(5), 2827–2836, doi:10.5194/acp-13-2827-2013, 2013.

646   Turro, N. J.: Influence of nuclear spin on chemical, reactions: Magnetic isotope and.magnetic field effects (A Review),
647   Proceedings of the National Academy of Science USA, 80, 609–621, 1983.

648   Wang, F., Saiz-Lopez, A., Mahajan, A. S., Gomez Martin, J. C., Armstrong, D., Lemes, M., Hay, T. and Prados-
649   Roman, C.: Enhanced production of oxidised mercury over the tropical Pacific Ocean: a key missing oxidation
650   pathway, Atmospheric Chemistry and Physics, 14(3), 1323–1335, doi:10.5194/acp-14-1323-2014, 2014.

651   Wang, Z., Chen, J., Feng, X., Hintelmann, H., Yuan, S., Cai, H., Huang, Q., Wang, S. and Wang, F.: Mass-dependent
652   and mass-independent fractionation of mercury isotopes in precipitation from Guiyang, SW China, Comptes Rendus
653   Geoscience, 347(7), 358–367, doi:https://doi.org/10.1016/j.crte.2015.02.006, 2015.

654   Weiss-Penzias, P., Amos, H. M., Selin, N. E., Gustin, M. S., Jaffe, D. A., Obrist, D., Sheu, G. R. and Giang, A.: Use
655   of a global model to understand speciated atmospheric mercury observations at five high-elevation sites, Atmospheric
656   Chemistry and Physics, 15(3), 1161–1173, doi:10.5194/acp-15-1161-2015, 2015.

657   Wiederhold, J. G., Cramer, C. J., Daniel, K., Infante, I., Bourdon, B. and Kretzschmar, R.: Equilibrium mercury
658   isotope fractionation between dissolved Hg(II) species and thiol-bound Hg, Environmental Science and Technology,
659   44, 4191–4197, 2010.

660   Yang, X., Jiskra, M. and Sonke, J. E.: Experimental rainwater divalent mercury speciation and photoreduction rates
661   in the presence of halides and organic carbon, Science of The Total Environment, 697, 133821,
662   doi:https://doi.org/10.1016/j.scitotenv.2019.133821, 2019.

663   Zheng, W. and Hintelmann, H.: Mercury isotope fractionation during photoreduction in natural water is controlled
664   by its Hg/DOC ratio., Geochimica et Cosmochimca Acta, 73, 6704–6715, 2009.

665   Zheng, W. and Hintelmann, H.: Isotope Fractionation of Mercury during Its Photochemical Reduction by Low-
666   Molecular-Weight Organic Compounds, Journal of Physical Chemistry A, 114, 4246–4253, 2010.

667

668

669

670

671 **Table 1. Mean Δ^{200}Hg signatures for Hg emissions and atmospheric reservoirs.** Mean and 1σ for

672 published rainfall data represents the mean of means of remote site data points for each study in order to avoid

673 site type and sample number bias. Global GEM emission Δ^{200}Hg was calculated from the listed Hg fluxes and

674 modeled Δ^{200}Hg. The combined uncertainty on calculated atmospheric GEM and RM fractions was

675 propagated from uncertainties on observational data for emissions and RM and GEM Δ^{200}Hg.

Sample type	Hg flux	Δ^{200}Hg	1σ	
	Mg y^{-1}	‰	‰	
Pic du Midi RM		0.15	0.12	This study
Rainfall Hg		0.13	0.06	(Blum et al., 2014; Demers et al., 2013; Enrico et al., 2016; Gratz et al., 2010; Motta et al., 2019; Obrist et al., 2017; Sherman et al., 2012; Wang et al., 2015)
Pic du Midi GEM		-0.03	0.02	This study, (Fu et al., 2016b)
Ocean GEM emission	4600	0.03		(Horowitz et al., 2017; Sun et al., 2019)
Anthropogenic GEM	1470	0		(Horowitz et al., 2017; Sun et al., 2019)
Soil GEM emission	1420	-0.02		(Horowitz et al., 2017; Sun et al., 2019)
Volcanic GEM emission	250	0		(Horowitz et al., 2017; Sun et al., 2019)
Global GEM emission	7740	0.02	0.02	(Horowitz et al., 2017; Sun et al., 2019)
f(RM)		0.30[a]	0.17	
f(GEM)		0.70[a]	0.17	

676 [a] calculated from mass balance: Δ^{200}Hg(global GEM emitted) = f(RM) × Δ^{200}Hg(rainfall) + f(GEM) ×

677 Δ^{200}Hg(PDM GEM), and f(RM) + f(GEM) = 1

678

679

680 **Figure 1. Hg speciation and isotope variability during a free tropospheric air mass intrusion.** From 20 to

681 28 Dec 2012, high frequency (12h, 24h) gaseous elemental Hg^0 (GEM) isotope signatures δ^{202}Hg, Δ^{199}Hg,

682 Δ^{200}Hg (A), CO and O$_3$ concentrations (B), atmospheric GOM, PBM and GEM concentrations (C), and solar

683 radiation and relative air humidity (D) showed a 48h long intrusion of a free tropospheric air mass, high in

684 GOM, and low in GEM and humidity.
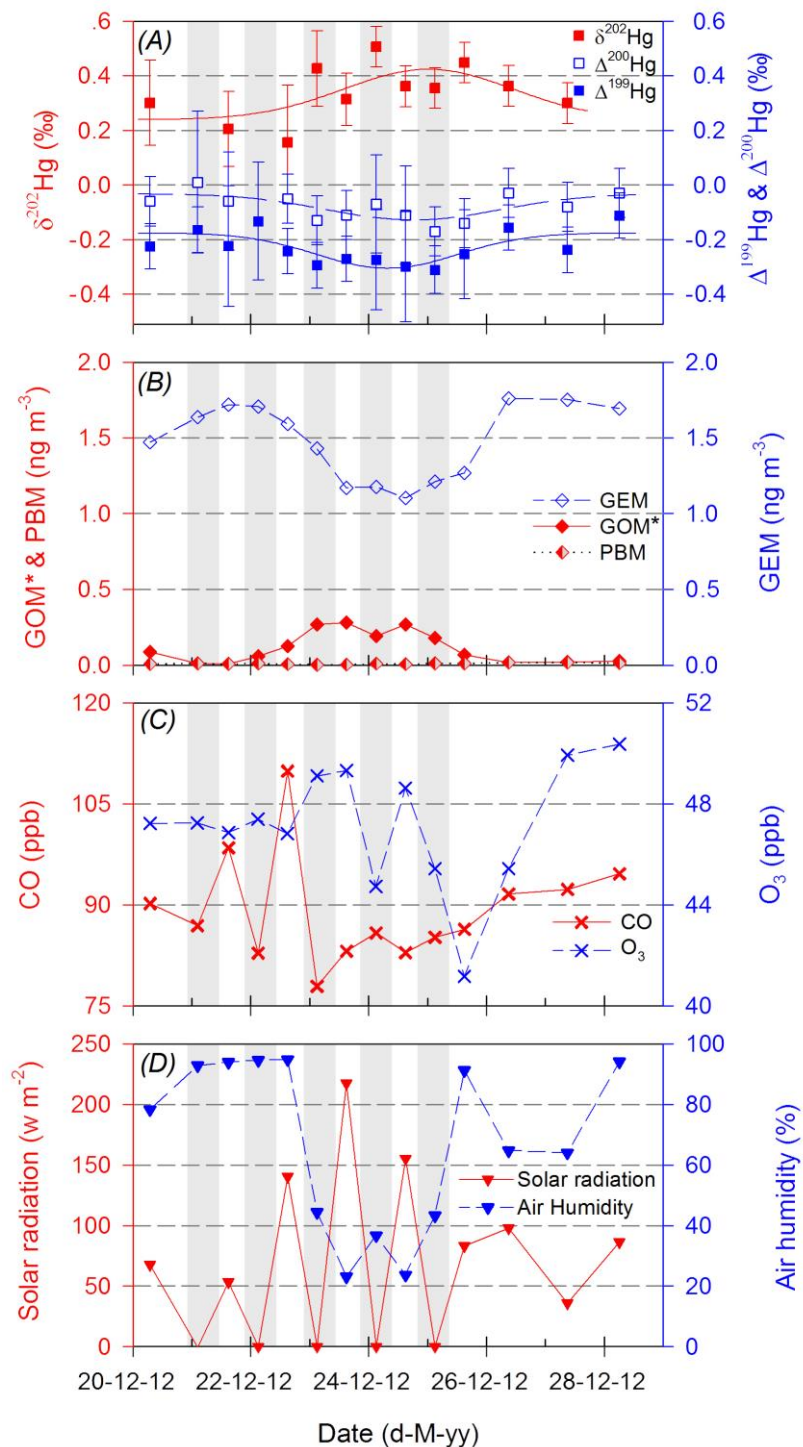
685

686

687 **Figure 2. Air mass back-trajectories of the free tropospheric air mass intrusion.** 7-day backward

688 trajectories of the high frequency (12h, 24h) gaseous elemental Hg^0 (GEM) isotope samples obtained from 20

689 to 28 Dec 2012: Travelling height (A, indicated by air pressure), air mass humidity (B), solar radiation (C),

690 and air temperature (D). Date and time labels are mid-points of 12h and 24h Hg isotope sampling windows.
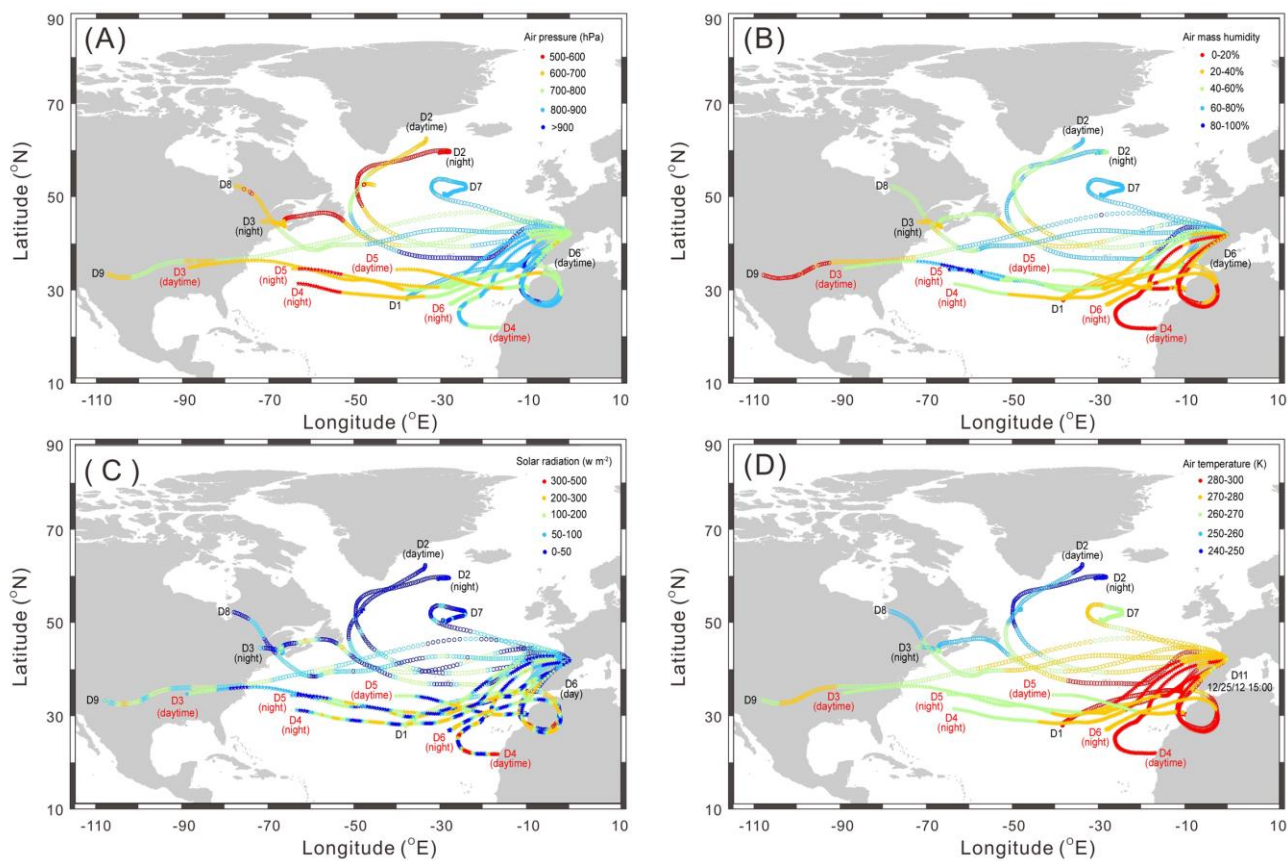

691

692 **Figure 3. Atmospheric Hg stable isotope variation at the Pic du Midi.** Hg mass dependent (δ^{202}Hg) and mass

693 independent (Δ^{199}Hg, Δ^{200}Hg, Δ^{201}Hg, Δ^{204}Hg) isotope signatures in reactive Hg (RM=GOM+PBM), cloud

694 water, 12h/24h GEM from this study, and previously published GEM (Fu et al., 2014) and rainfall (Enrico et

695 al., 2016).
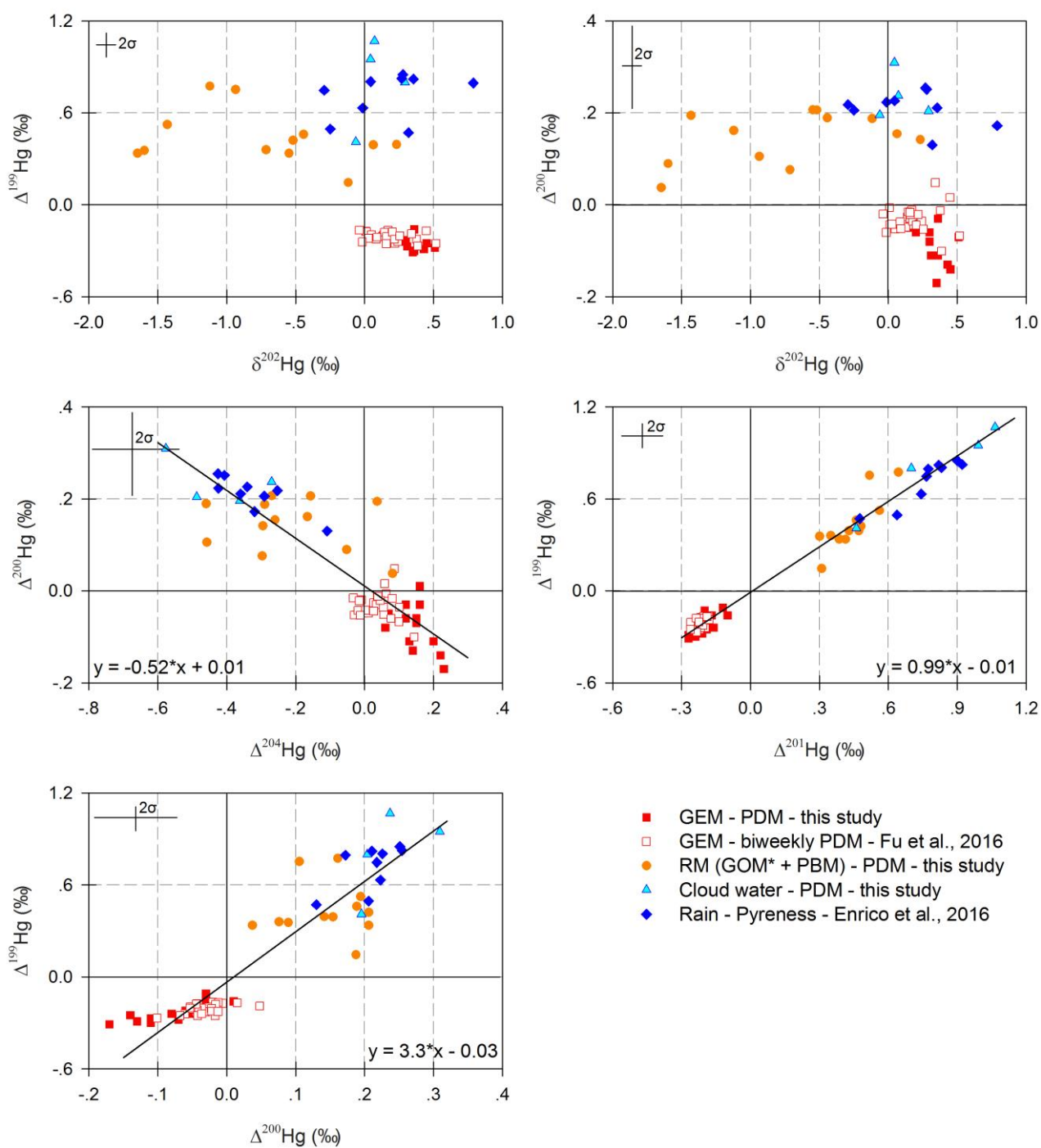
696

697

698 **Figure 4. Δ^{196}Hg measurement of rainfall.** A 20.5L rainfall sample containing 6.0 ng L^{-1} of Hg was pre-
699 concentrated 1200x to deliver a 0.015V signal on ^{196}Hg. The resulting Δ^{196}Hg signature is -0.06 ± 0.19‰ (2σ,
700 n=2) suggesting that nuclear self-shielding is not the underlying cause of atmospheric even-Hg MIF. A Δ^{202}Hg
701 of 0 is indicated in the graph, since the Δ^{xxx}Hg (where xxx are Hg isotopes masses 196 to 204) are calculated
702 relative to $\delta^{202/198}$Hg ratios, themselves anchored to the ^{198}Hg reference isotope.
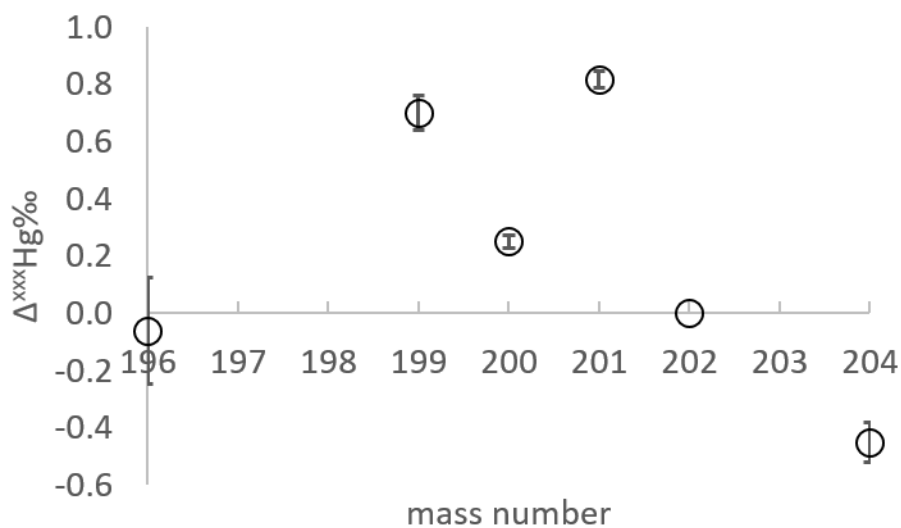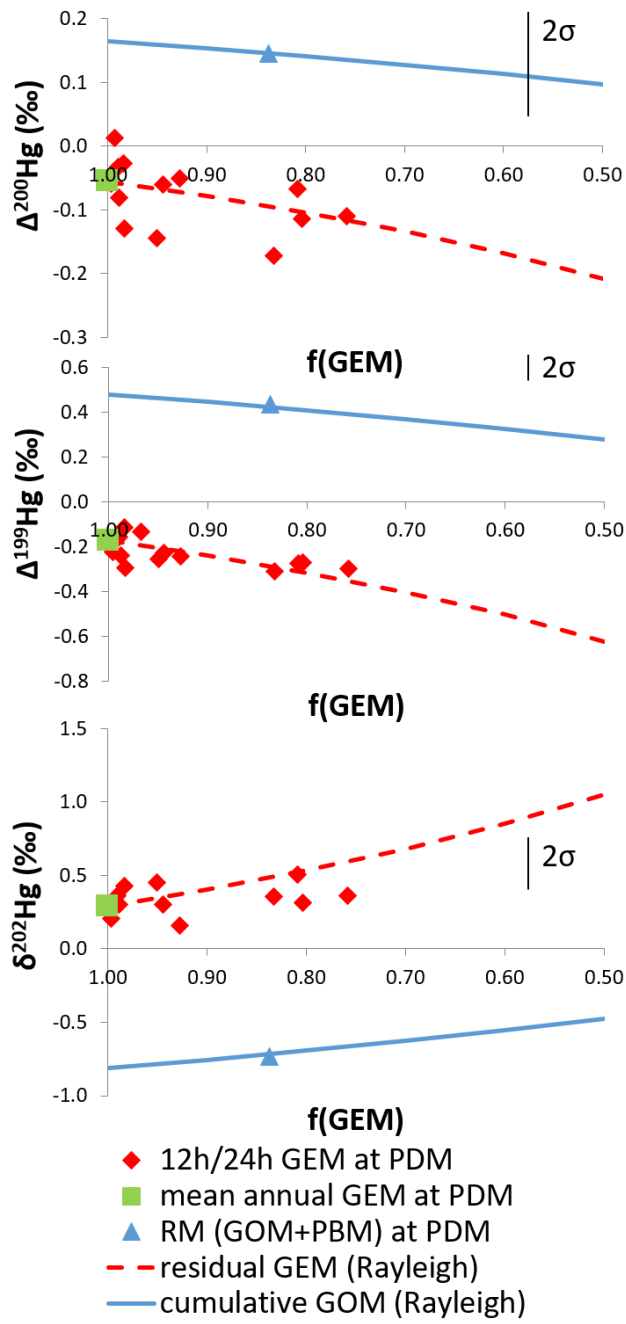

703
704

705 **Figure 5. Hg oxidation mass balance in free tropospheric air at the Pic du Midi.** Relationship between
706 gaseous elemental Hg[0] (GEM, ng m^{-3}) and gaseous oxidized Hg[II] (GOM*, ng m^{-3}) observed during the nine day
707 sampling campaign at PDM. Black circles and grey diamonds are Tekran GEM and GOM* data (Extended
708 Data), where grey diamonds represent the high GOM event only. A slope of -1 is indicative of Hg mass
709 conservation during GEM oxidation to GOM in the observed air mass. The uncorrected GOM*/GEM slope of
710 -0.44 is biased low due to latitudinal bias in the GEM precursor to GOM (see main text). Latitude corrected
711 subtropical Atlantic Ocean GEM levels (grey square) indicate a slope of -0.88, suggesting that Hg mass has
712 been conserved in the high GOM air mass detected at PDM.
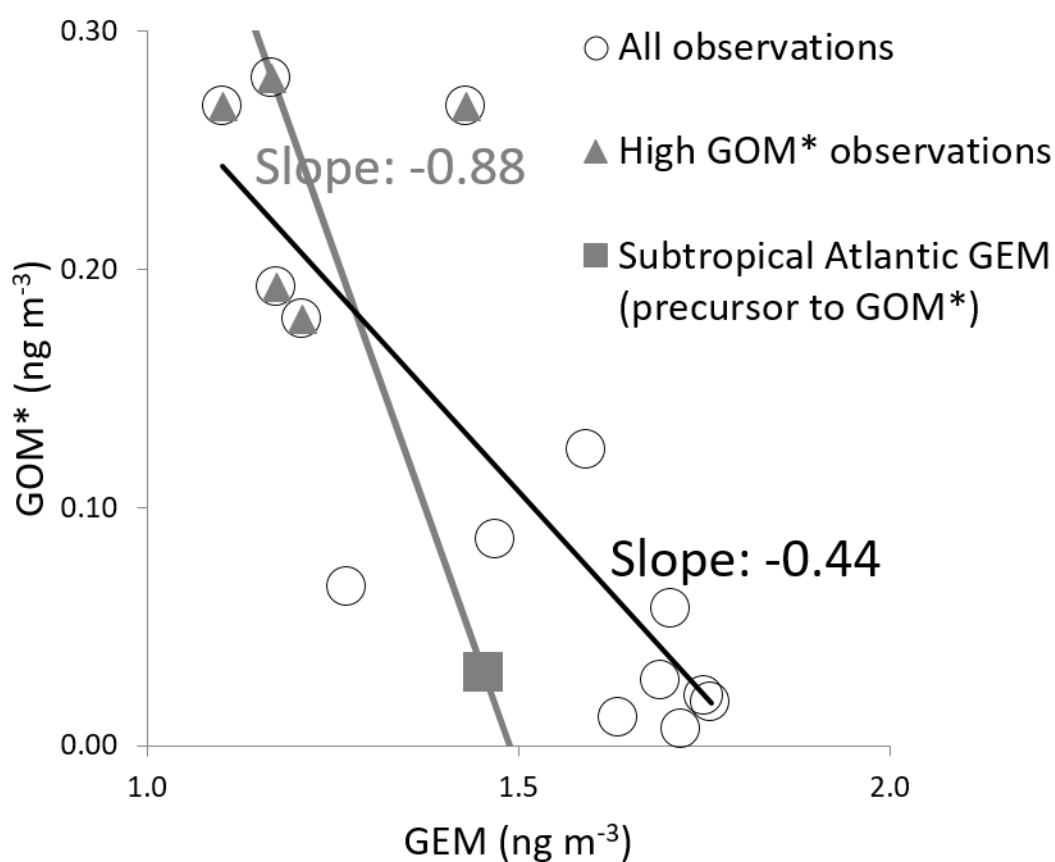
713
714
715

716 **Figure 6. Rayleigh diagrams for Hg isotope fractionation during Hg⁰ net oxidation.** This dataset is a

717 composite of GEM isotope composition (red diamonds) recorded in the Atlantic Ocean free tropospheric air

718 mass intrusion at PDM in Dec 2012, and mean RM (=GOM*+PBM ~ GOM*) isotope composition (blue

719 triangles) at PDM recorded from June – October 2014. Isotope fractionation factors $\varepsilon^{\delta 202}_{MDF(GOM-GEM)}$ of -1.1 $\pm$

720 0.2‰, $\varepsilon^{\Delta 199}_{MIF(GOM-GEM)}$ of 0.65 $\pm$ 0.11‰, $\varepsilon^{\Delta 200}_{MIF(GOM-GEM)}$ of 0.22 $\pm$ 0.05‰, $\varepsilon^{\Delta 201}_{MIF(GOM-GEM)}$ of 0.65 $\pm$ 0.10‰, and

721 $\varepsilon^{\Delta 204}_{MIF(GOM-GEM)}$ of -0.39 $\pm$ 0.12‰ (all 1SE) were fitted by log-linear regression of Rayleigh equations for residual

722 GEM and cumulative GOM*. All 12h and 24h observations (blue diamonds) over the nine day period were

723 included in the fitting. The starting isotopic composition (green square) is the mean annual GEM composition

724 at PDM (Fu et al., 2016b).

725
726

28